Electronic Supplementary Material (ESI) for ChemComm.
This journal is © The Royal Society of Chemistry 2020

Supporting information

Molecular Dopant Determines the Structure of a Physisorbed Self-Assembled Molecular Network

Roelof Steeno,[a] Andrea Minoia,[b] Maria C. Gimenez-Lopez,[c,d] Matthew Blunt,[e] Neil R. Champness,[c] Roberto Lazzaroni,[b] Kunal S. Mali,[a] and Steven De Feyter[a]

[a]Division of Molecular Imaging and Photonics, Department of Chemistry, KU Leuven, Celestijnenlaan 200F, B-3001 Leuven, Belgium, [b]Laboratory for Chemistry of Novel Materials, University of Mons, Place du Parc 20, 7000 Mons, Belgium, [c]School of Chemistry, University of Nottingham, Nottingham, NG7 2RD, UK, [d]Centro Singular de Investigacion en Quimica Biolóxica e Materiais Moleculares (CiQUS), Universidade de Santiago de Compostela, 15782 Santiago de Compostela, Spain, [e]Department of Chemistry, University College London, 20 Gordon Street, London, WC1H 0AJ, UK.

Experimental section

TPTC (99.9%, 2 equivalents of DMF) was used as received from Sigma Aldrich. Nonanoic acid (> 98%) was acquired from TCI Europe N.V. and used without further purification. In-house synthesized **TPTC** was made following a reported procedure (also see below).[1] A saturated solution of **TPTC** was made by weighing 2 mg of **TPTC** and 2 mL of nonanoic was added to it. The solution was left to equilibrate for one week. About 20 µL of the saturated solution (supernatant) was drop casted on freshly cleaved HOPG (ZYB grade, Advanced Ceramics Inc.) prior to STM imaging. For annealing experiments, after drop casting the solution, the HOPG substrate contained in a glass petri dish was placed on a hot plate. The plate was heated to 60 °C. After the hot plate reached 60 °C, the temperature was maintained for 60 seconds and then the hot plate was turned off. The sample was left on the hot plate for additional 15 minutes to allow it to cool down to room temperature. STM imaging was realized at room temperature (20-22 °C) in constant current mode with a PicoLE (Keysight) machine using mechanically cut Pt/Ir (80%/20%) tips with a diameter of 0.25 mm. For regular STM imaging, a tunneling current and sample bias of ~ 0.05 nA and ~–0.8 V was applied. To remove the second layer of **TPTC**, the tunneling current was increased to 0.3 nA while keeping the sample bias constant for one scan. STM data was processed using Scanning Probe Imaging Processor (SPIP 6.3.5) software from Image Metrology ApS.

Possible origin of impurity and alternative synthetic strategy for decreasing the extent of it

The synthesis of such systems typically uses a Pd catalyzed cross coupling reaction between 1,4-dibromobenzene and a boronic acid functionalized derivative of isophthalic acid (see below). However, dimerization of the dibromobenzene is possible under reaction conditions which yields 4,4'-dibromo-1,1'-biphenyl. This side product then reacts with the isophthalic acid derivative to yield **QPTC**. The formation of larger units is possible as well with the same homocoupling occurring more than once.[2, 3] We believe that the commercial sample was obtained using this protocol and thus is prone to the presence of small percentage of **QPTC** impurity.

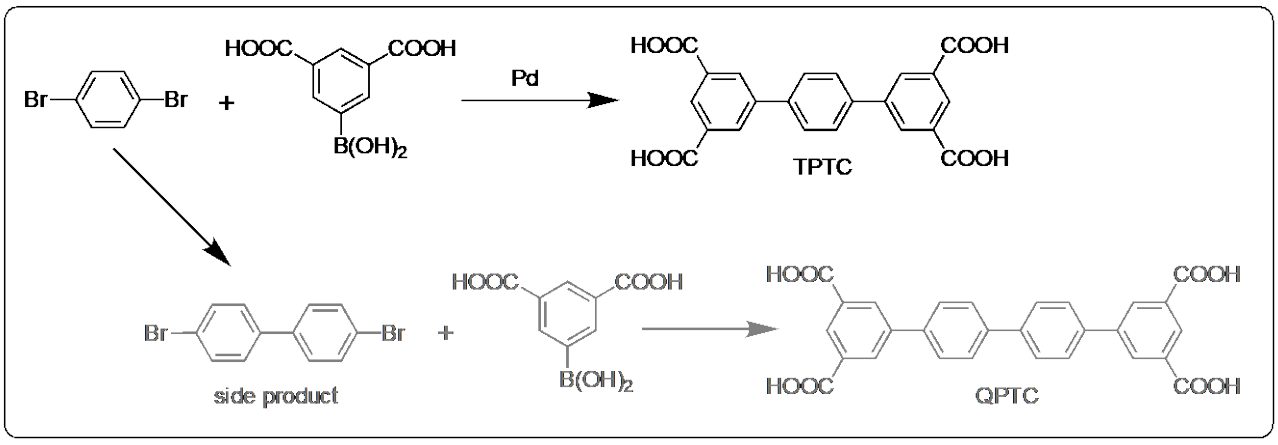

The in-house synthesis of **TPTC** was carried out by following a different synthetic strategy. First, Pd catalyzed cross coupling was carried out by reacting a 1,3-dimethly-(5-boronic acid)-benzene with 1,4-dibromobenzene. The product of this reaction was purified prior to oxidation to the corresponding tetra-acid. Purification of this intermediate by column chromatography is easier than that of the final product due to the lower polarity of the intermediate (see below, also for details see reference 1).

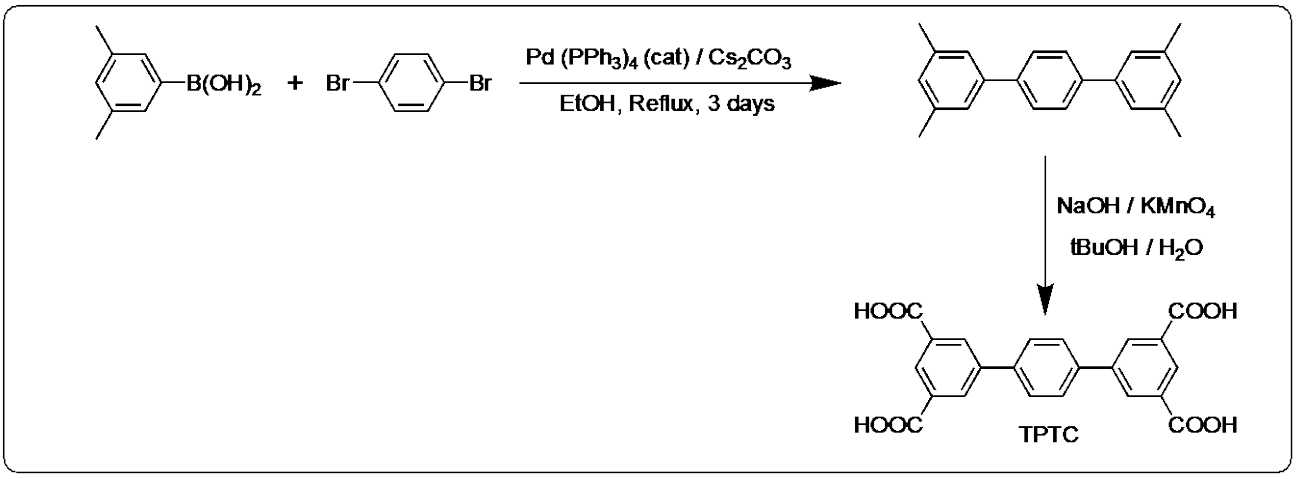

NMR and ESI-MS characterization of the commercial and the pure TPTC samples

NMR :

^{1}H NMR (600 MHz) were collected for both commercial and 'pure' samples of TPTC. We note that the ^{1}H NMR spectra for TPTC and QPTC (or QQPTC) are anticipated to be near identical, based on simple calculations regarding the number of peaks, and this is indeed observed in the recorded spectra. It is notable that the commercial sample is shown to contain N,N-dimethylformamide and signals associated with this molecule are observed in the spectrum (notably at 7.96 ppm). On the contrary to ^{13}C NMR, ^{1}H NMR can be used as quantitative tool. Here below the ^{1}H NMR spectra for the pure and commercial sample are shown to illustrate the similarities between the two samples.

^{1}H NMR pure TPTC

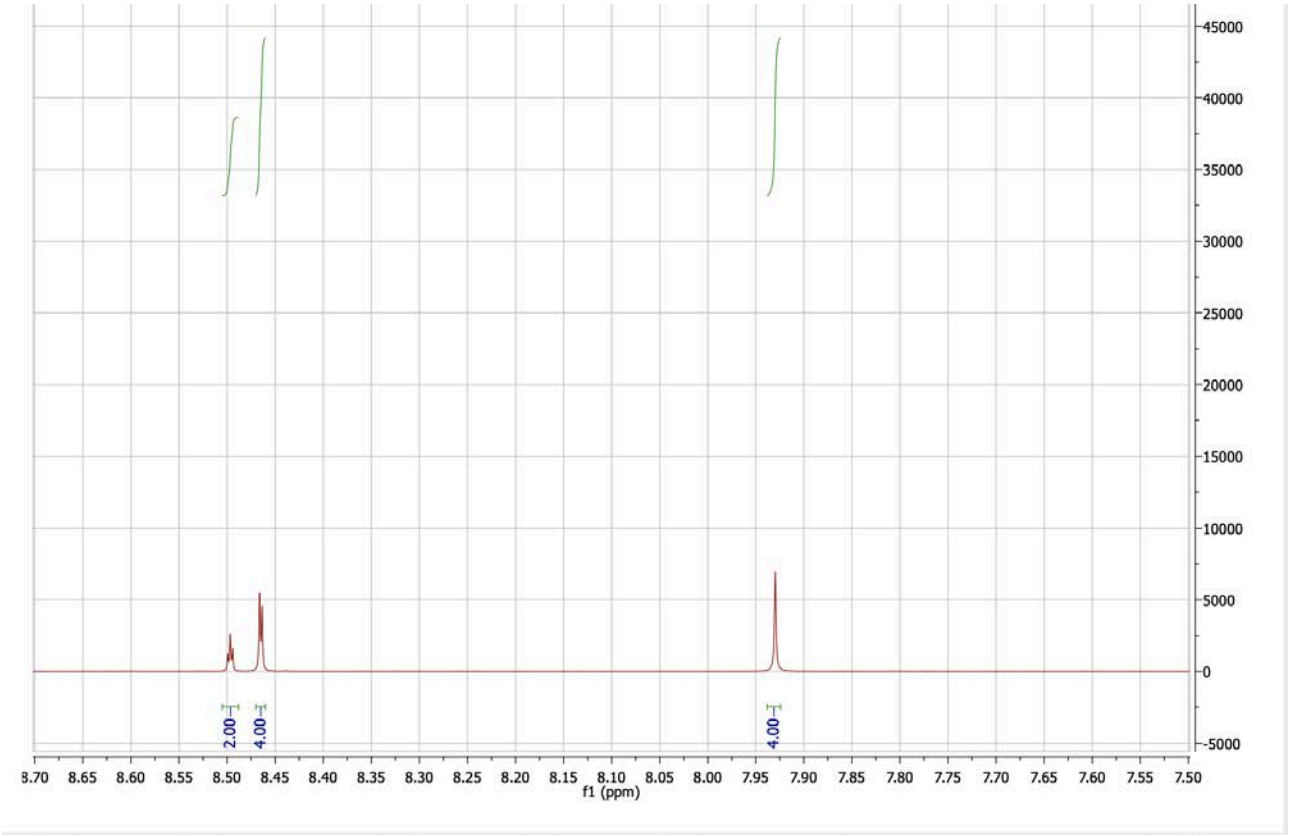

^{1}H NMR commercial (impure TPTC)

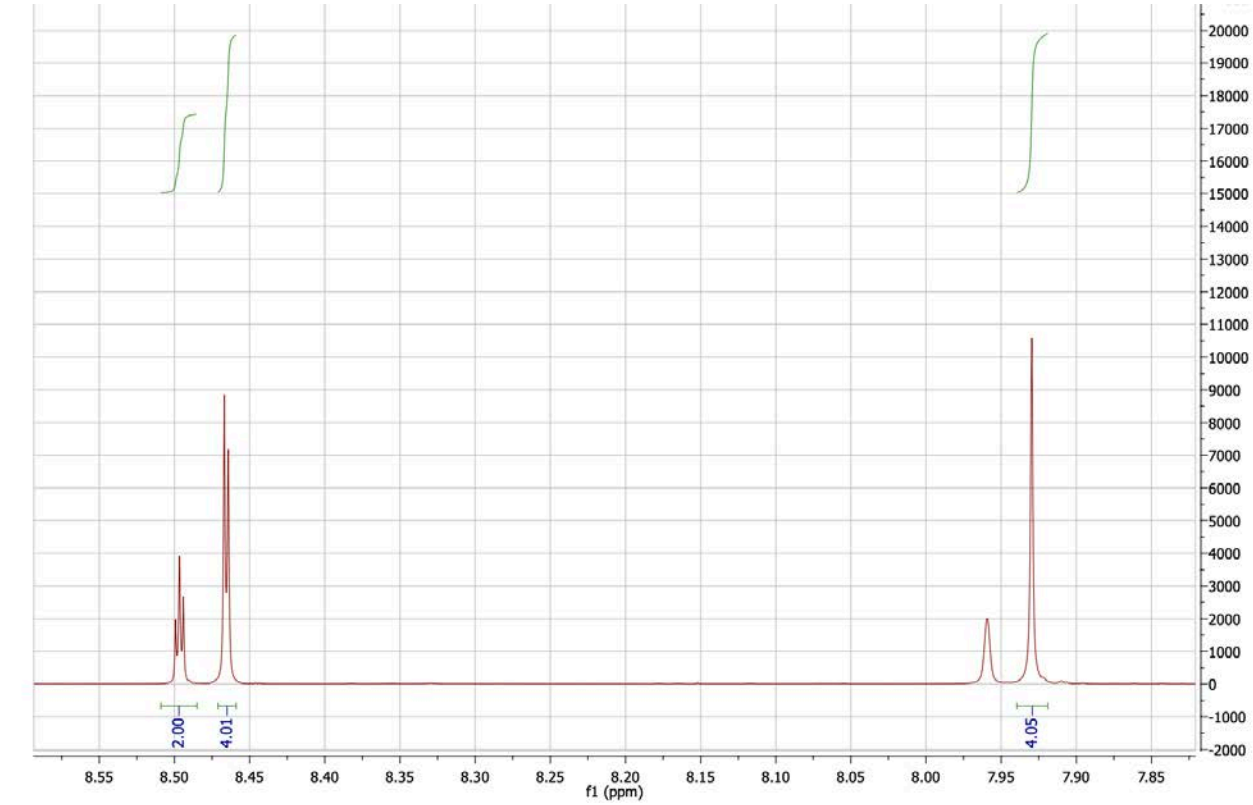

By careful evaluation of the ^{1}H NMR spectrum and comparison of the integration of the peak at 7.925 in the commercial sample and that in the pure TPTC one can estimate that there is approximately 2.5 % of QPTC in the commercial sample. We also note that this quantification is prone to large errors

ESI-MS:

To ascertain that the difference observed on the peak integration (2.5 %) after comparing both samples is mainly due to the presence of QPTC, electrospray ionization-mass spectrometry (ESI-MS) was carried out on the "pure" and compared with the commercially obtained TPTC samples. ESI-MS data shows the presence of QPTC in the commercial sample, as indicated by the peak seen at 481 m/z (TPTC is seen at 405 m/z). Although this is not quantitative, the mass spectra confirm the presence of QPTC which is not observed in the pure TPTC sample. The ESI-MS spectra are shown below to illustrate the differences between the two samples.

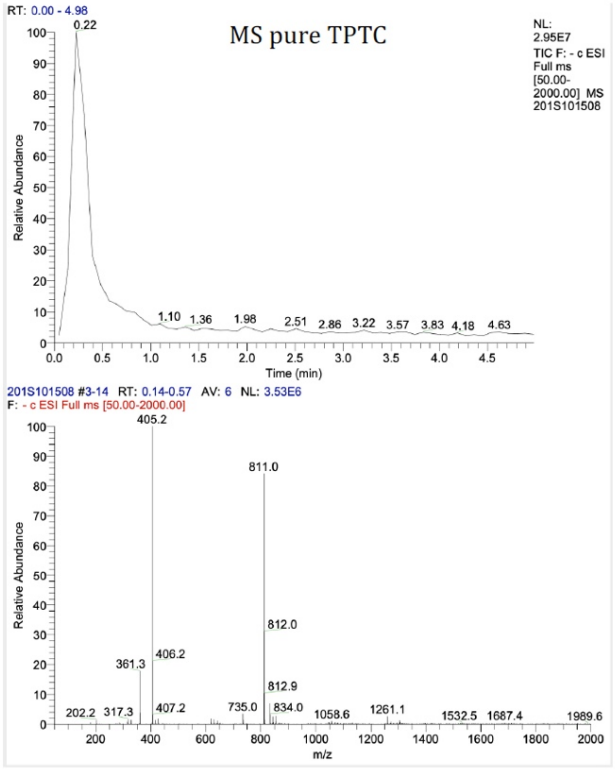

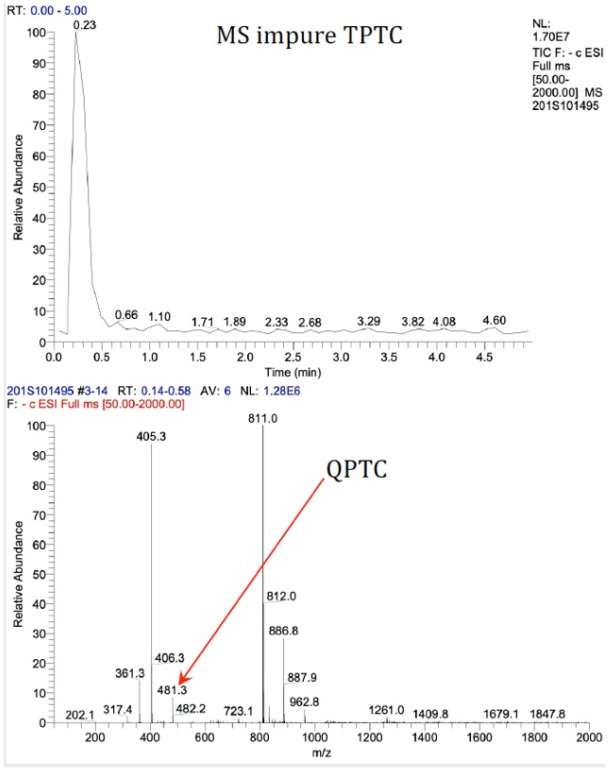

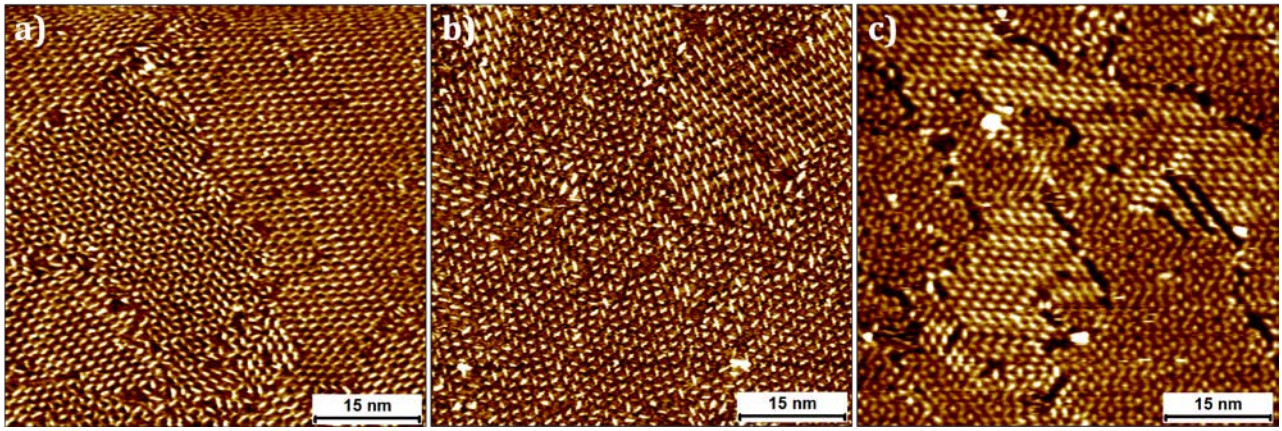

Fig. S1. STM images showing the co-existence of the parallel and the random phase at the nonanoic acid/HOPG interface. Monolayers were obtained from (a) Saturated solution (b) 10% dilution from saturated solution (c) 50% dilution from the saturated solution. We noted that the percentage surface area occupied by the parallel phase at lower concentrations was reduced relative to that observed in the case of saturated solutions.

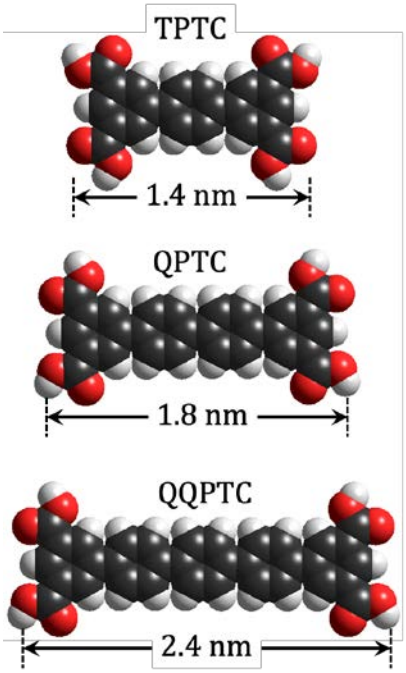

Fig. S2. Molecular models showing the length of the building blocks.

Computational details

Molecular Modeling simulations have been used to investigate the relative stabilities of both ordered (parallel phase) and disordered TPTC and QTPC phases on graphite, due to the interplay of molecular shape and size with the range of intermolecular H-bonds bonding neighboring molecules. Models have also been used to investigate the monolayer's ability, or lack of, to template the growth of the layer on top of it. It should be noted here that the solvent has not been taken into consideration in these models,

as the experimental results do not show solvent molecules to be playing an active role in the stability and templating abilities for the H-bonded supramolecular networks formed by TPTC and QPTC molecules.

The adsorption behavior of single molecules as well as that of the self-assembled networks on graphite surface was investigated using molecular mechanic calculations. All simulations have been carried out with the Biovia Materials Studio 2018 molecular modeling package.

Since intermolecular H-bonding interactions play a crucial role in the formation and stabilization of the supramolecular self-assembly, for the atomistic simulations were carried out with the Dreiding Force field, which comprises an explicit hydrogen bond term. Gasteiger charges were used as atomic charges for the **TPTC** and **QTPC** molecules. A single, periodic, layer of graphite was used as the surface and it was treated as a rigid body during the simulation. No atomic charges were assigned to the atoms on the graphite. The electrostatic interactions were calculated using Ewald Summation and a cutoff of 0.9nm was used for the Van Der Waals interactions.

Physisorption of single TPTC and QPTC molecules on surface

The molecular adsorption energy, E_{ads} in Eq. 1, is calculated as the energy difference between the energy of a single molecule adsorbed on the surface, E_{sys}, and the energy of the isolated molecule, E_{mol}.

$$E_{ads} = E_{sys} - E_{mol} \qquad (1)$$

Since graphite is considered as a rigid body, its internal energy is zero and it does not contribute to the molecular adsorption energy.

As expected, both **TPTC** and **QPTC** molecules adsorb flat on graphite, with the larger **QPTC** molecules having a stronger interaction with the surface than the smaller **TPTC** molecule (-63.7 kcal mol^{-1} *versus* d -52.0 kcal mol^{-1}, respectively).

Modeling QPTC and TPTC Supramolecular Self-Assembly

First, we set to understand why QPTC only forms regular self-assemblies with the molecules in a parallel orientation. In this assembly, all the molecules are linked together *via* the highly-directional intermolecular H-bonds, and the resulting H-bonding pattern is what stabilizes the self-assembly.

We then systematically tried to build a number of amorphous monolayers of **QPTC** under the constraint that molecules have to maximize the number of H-bonds formed with their neighbors. As Figure S3 illustrates, mismatches soon happen: because of their length, **QPTC** molecules in random orientation cannot form extended H-bonding networks.

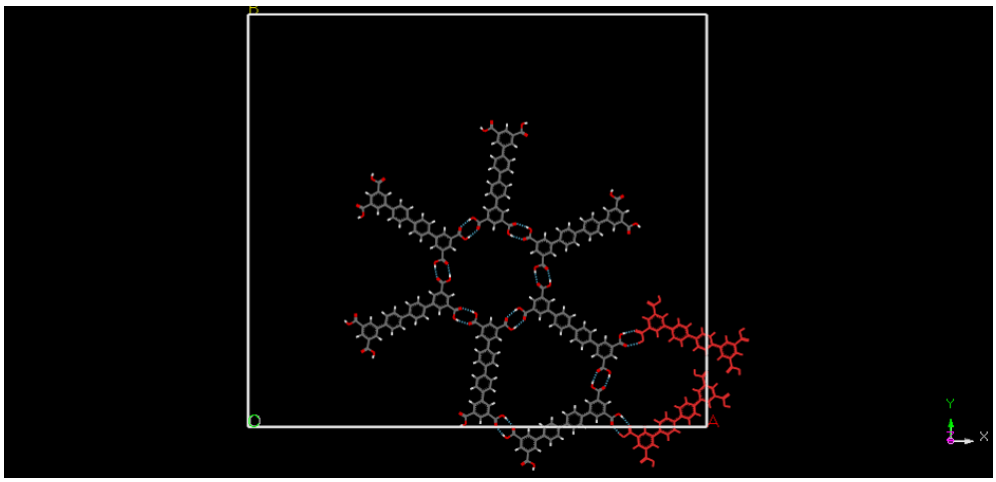

Fig S3. A molecular model showing the inability of QPTC to assemble in a random tiling network.

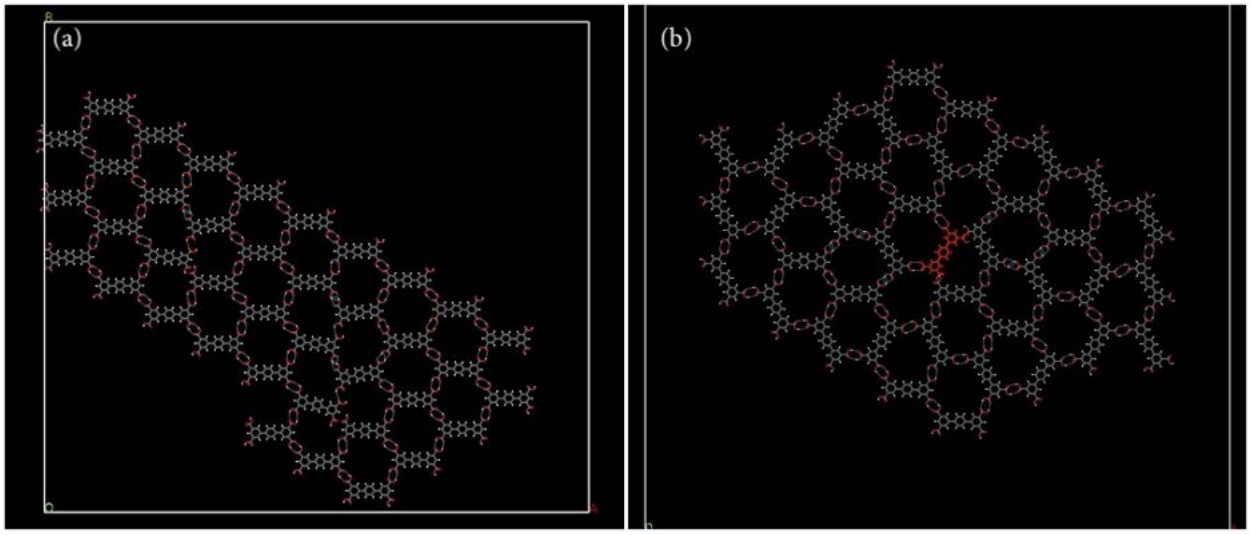

Fig S4. Molecular models showing the ability of **TPTC** to assemble either into a parallel (a) or a random tiling network (b).

For **TPTC** molecules, both assemblies shown in Figure S4 include 39 molecules. Within the random tiling network, the molecules can form H-bonds with no structural deformation and only one molecule (red, b) was found to show a minor mismatch. The total potential energies of the two arrangements shown above were found be identical (parallel: –123.4 kcal mol^{-1}; random tiling network: –124.1 kcal mol^{-1}).

STM data showing the transition of the parallel phase to the random tiling network

The area of parallel domains (highlighted in blue) was measured using the Scanning Probe Imaging Processor (SPIP 6.3.5) software. Dividing the area covered by the parallel domains by the total area of the image (at least 60 x 60 nm^2) yielded the percentage of the surface covered by parallel domains. The decrease in surface coverage of the parallel phase with time, as shown in Fig. 3c in the main text, was determined by performing this analysis at different points in time.

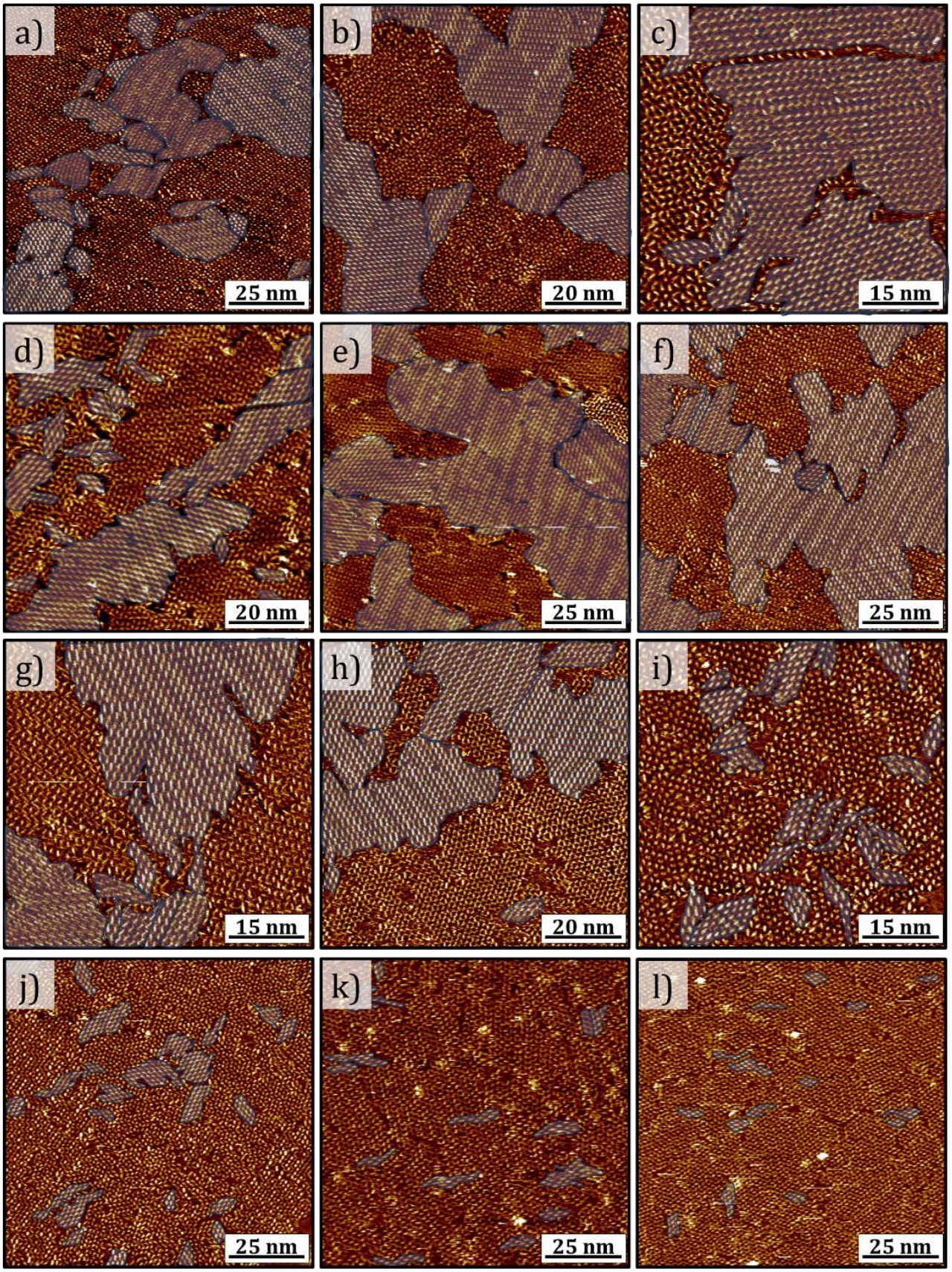

Fig. S5. Representative STM dataset showing a decrease in the surface coverage of the parallel phase and increase in that of the random phase as a function of time. STM images (60 × 60 – 100 × 100 nm^2) used to calculate the surface coverage at different times (hours): (a) 0.38, (b) 0.87, (c) 1.02, (d) 1.42, (e) 4.33, (f) 4.68, (g) 4.95, (h) 5.4, (i) 6.72, (j) 7.13, (k) 7.67 and (l) 7.98.

STM data showing the change in the surface composition of the monolayer over time

The depletion of impurity molecules with time, as shown in Fig. 3d, was obtained from calculation the relative coverage of each component at different times.

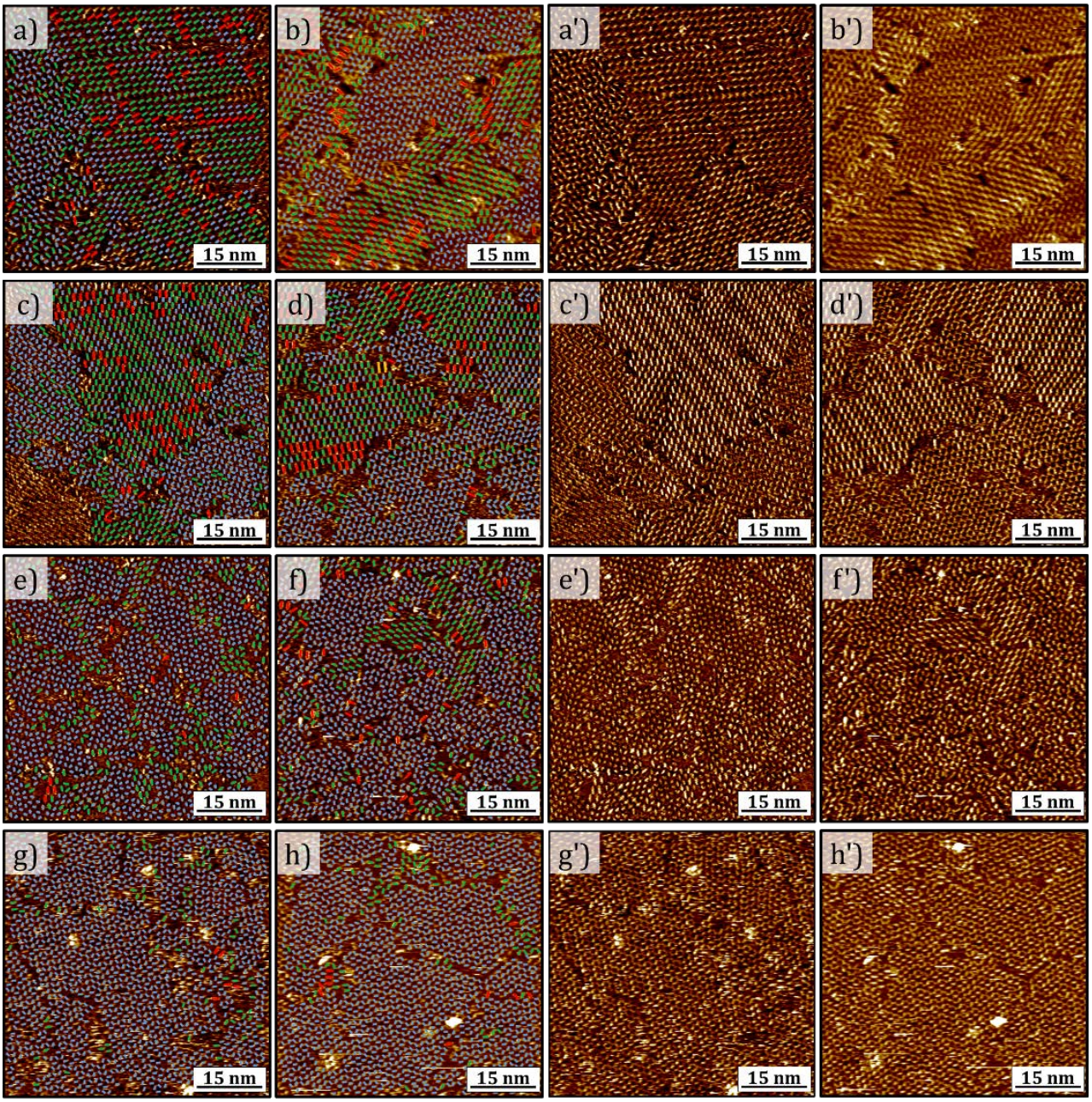

Fig. S6. Representative STM dataset showing the gradual removal of the **QPTC** (green) from monolayer which is associated the incorporation of adsorption of **TPTC** (blue). 60 × 60 nm^2 STM images with and without (') mask used to calculate the coverage (%) of each component at times (hours): (a) 1.02, (b) 1.42, (c) 4.97, (d) 5.4, (e) 6.72, (f) 7.13, (g) 7.67 and (h) 7.98.

To obtain the relative coverage (%) of each component the following formula was applied.

$$\text{Coverage} = \frac{\text{Number of } \mathbf{TPTC}\text{, QPTC or 5}\mathbf{TPTC} \text{ molecules}}{\text{Number of } \mathbf{TPTC} \text{ molecules} + \left(4 * \frac{\text{Number of QPTC molecules}}{3}\right) + \left(5 * \frac{\text{Number of 5PTC molecules}}{3}\right)} * 100$$

Formation of bilayers after annealing

The growth of the bilayer induced by annealing of the sample is not clearly understood yet and needs further scrutiny. A local increase in the number of molecules adsorbing on top of the monolayer due to the evaporation of the solvent is mentioned in the main text. However, another possibility can also be considered. The solution may contain π-stacked aggregates and the annealing of the sample may break apart these stacks which cause a local increase in the solution concentration at increased temperature. As the temperature is lowered down to RT, these additional molecules adsorb onto the monolayer leading the growth of the bilayer.

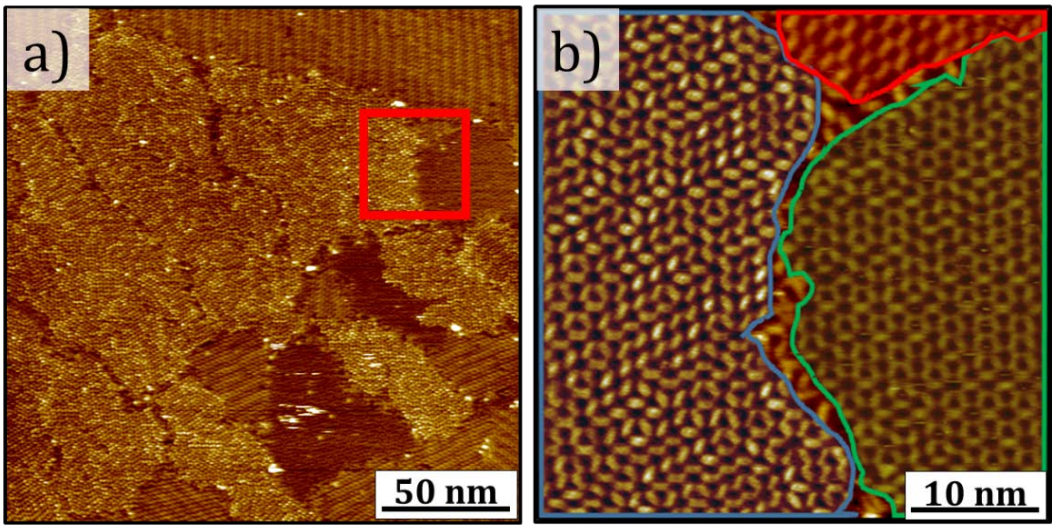

Fig. S7. STM images showing the growth of bilayers after annealing the samples at 60°C. (a) 200 × 200 nm² STM overview scan. (b) 40 × 40 nm² STM image highlighting a random monolayer (green), a random bilayer (blue) and parallel monolayer (red).

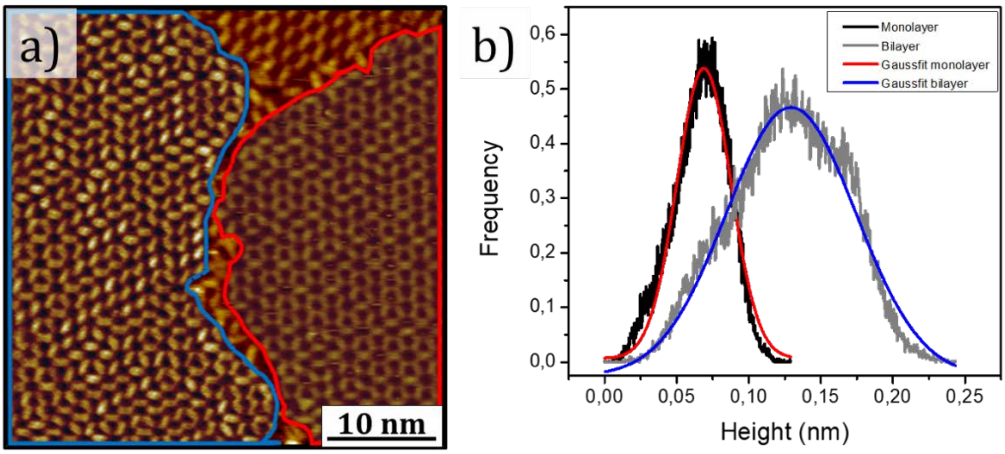

Fig. S8. Difference in the apparent height of the monolayer and bilayer domains. (a) 40 × 40 nm² STM image with a monolayer and bilayer domain highlighted respectively in red and blue. (b) Height histograms taken from the monolayer (black) and bilayer (gray) areas of the corresponding STM image. Gaussian curves were fitted through the histograms.

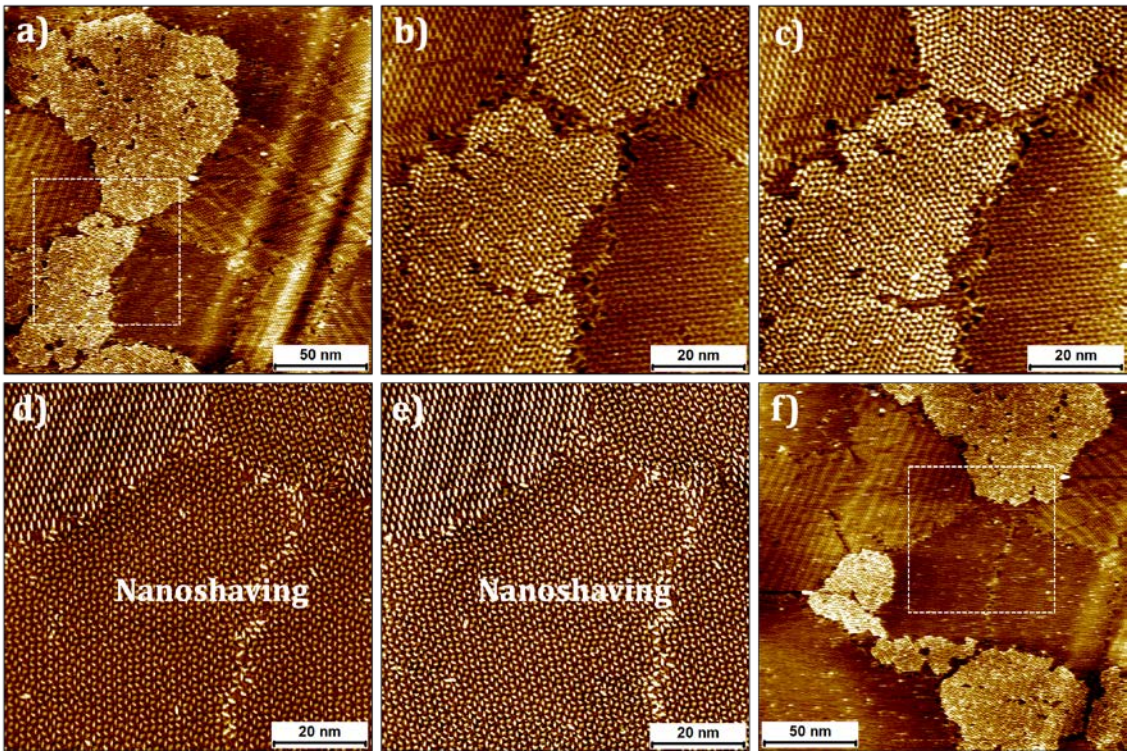

Fig S9. Large scale STM images showing the ability of STM to selectively remove the top layer of the bilayer assembly. Panel (a) shows a large-scale image in which large islands of bilayers can be seen. Panels (b, c) show the smaller scale image from the area highlighted in the white dotted square in panel (a). Panels (d, e) show the same area as in (b, c) but scanned at higher tunneling currents (I_{set} = 300 pA, V_{bias} = -800 mV) where the top layer is already removed. Panel (f) shows approximately the same area that was scanned at higher currents in earlier scans.

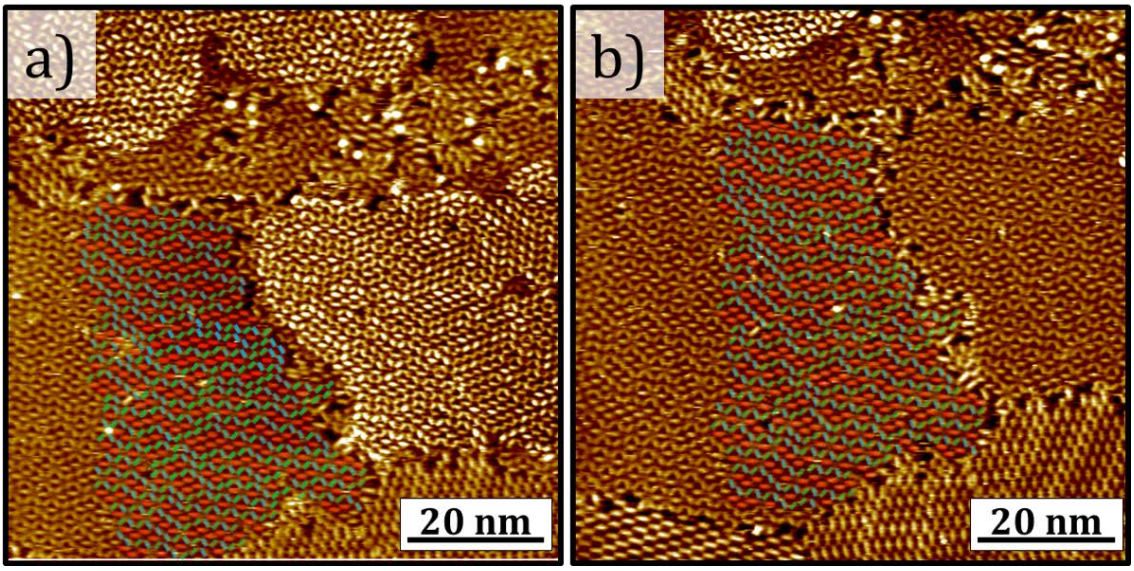

Fig. S10. The effect of the nanoshaving conditions. 80 × 80 nm^2 STM images (a) before and (b) after one scan at nanoshaving conditions (I_t = 0.3 nA, V_s = –0.8 V). After nanoshaving the bilayer's top layer is removed. The colored mask, with each color representing a different molecular orientation, shows the negligible impact of the nanoshaving conditions on monolayer domains.

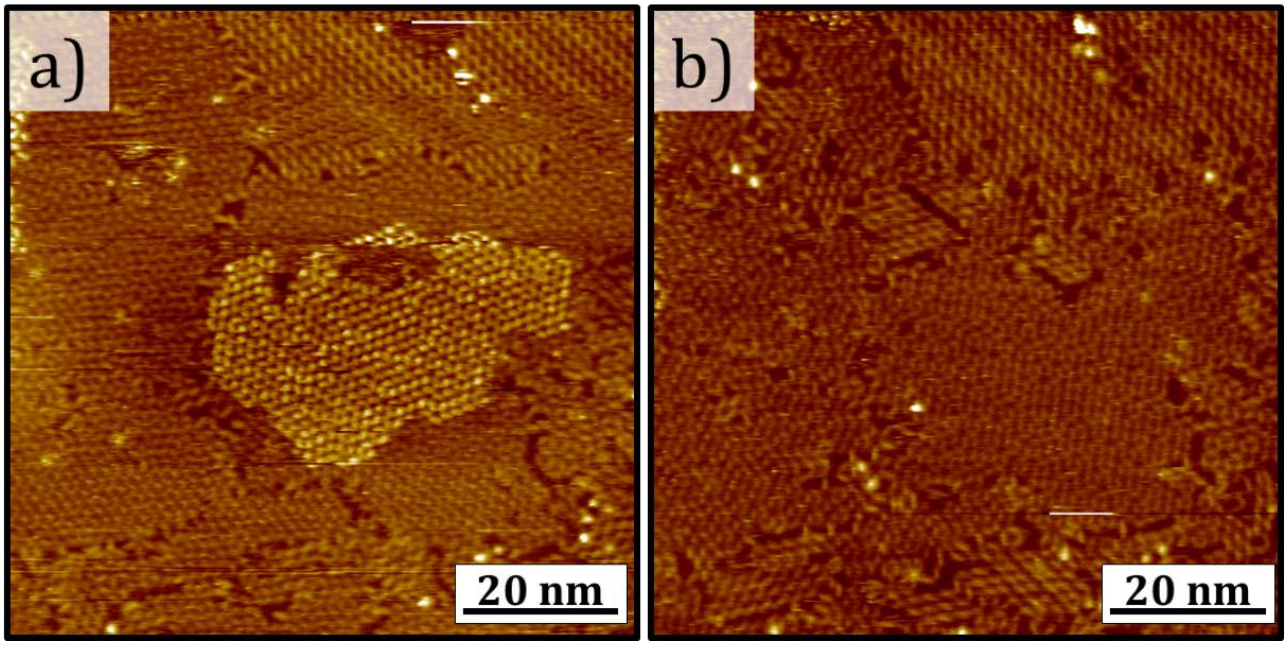

Fig. S11. STM image showing that no regrowth of bilayer is observed upon complete removal of the top layer. (a) before and (b) after nanoshaving.

Epitaxy of the top and the bottom layer of the random tiling bilayer

To correlate the position of molecules in the bilayer's top layer with the molecules in the bottom layer the following protocol was applied. In the first scan after nanoshaving shown in Fig. S8a, part of the bilayer's monolayer is exposed. As such, it is possible to overlay a mask on each molecule with a different color for each orientation. For the subsequent scans, where the bilayer slowly regrows, it is possible to fit the same mask to the image and add an additional mask (black) for the molecules in the top layer. Therefore, the relation between both masks can be determined and thus between the molecules.

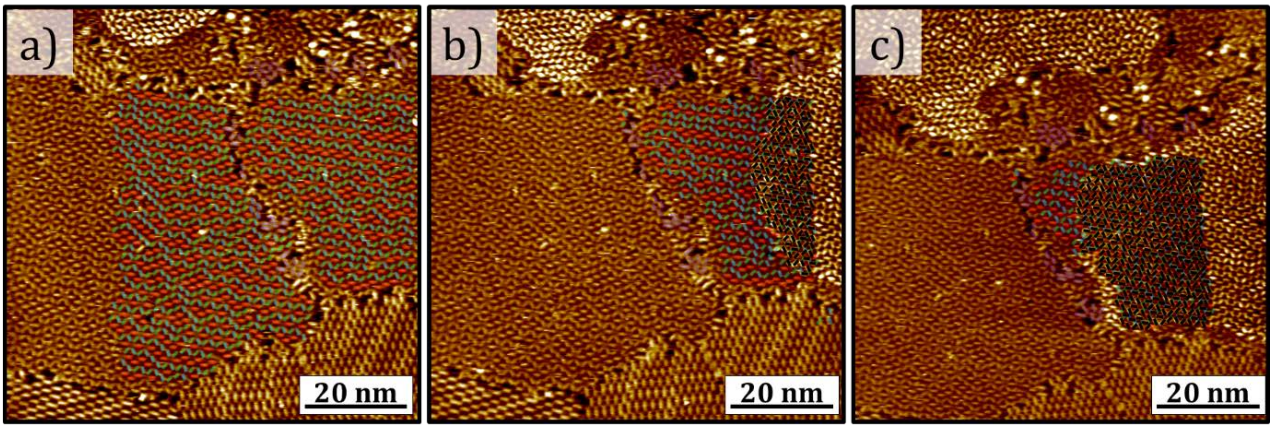

Fig. S12. Epitaxy of the top and the bottom layer of the random tiling bilayer. STM images obtained after (a) Immediately, (b) 3 minutes and (c) 10 minutes after nanoshaving. The purple overlayed rectangles were used as reference points between the images.

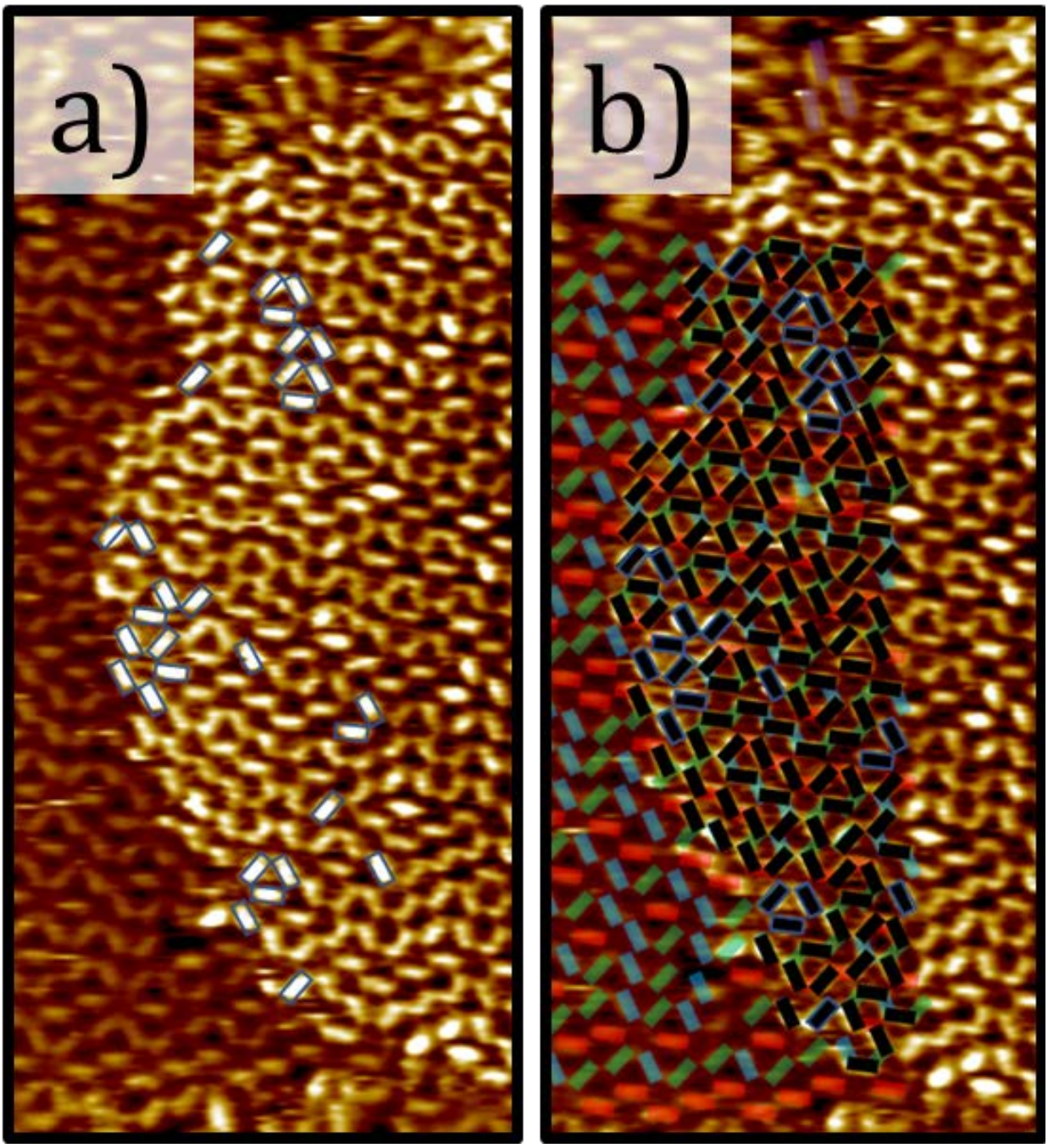

Fig. S13. Brighter contrast π-stacked bilayer molecules. STM image a) without and b) with rectangular masks for the bottom (red, green and blue) and the top (black) layer. The π-stacked molecules, are highlighted with a blue line.

The bilayer formation: Insight from molecular modelling

We use the modeling to investigate the mechanism leading to the formation of a **TPTC** layer atop the one formed on the graphite surface. In particular, we aim to (a) understand whether the bottom layer templates the growth of the top one and (b) why the **TPTC** molecules in the top layer are mostly

adsorbed on top of the H-bonded carboxyl moieties, rather than be adsorbed atop the terphenyl backbone of the molecules in the bottom layer.

In order to check whether the bottom layer templates the growth of the top layer, we assume the molecules in the top layer should find strong preferential adsorption sites when interacting with the **TPTC** monolayer below. There are two main ways a molecule on a top layer can interact with the **TPTC** molecules below: (i) by adsorbing atop a **TPTC** molecule in the bottom layer, resulting in a superposition of their terphenyl backbones, or (ii) by sitting atop the H-bonded carboxyl moieties of two interacting **TPTC** molecules in the bottom layer. These arrangements are illustrated in Figure S14 for a molecule interacting with the arrow head dimer below. The same is true if we use the parallel dimer.

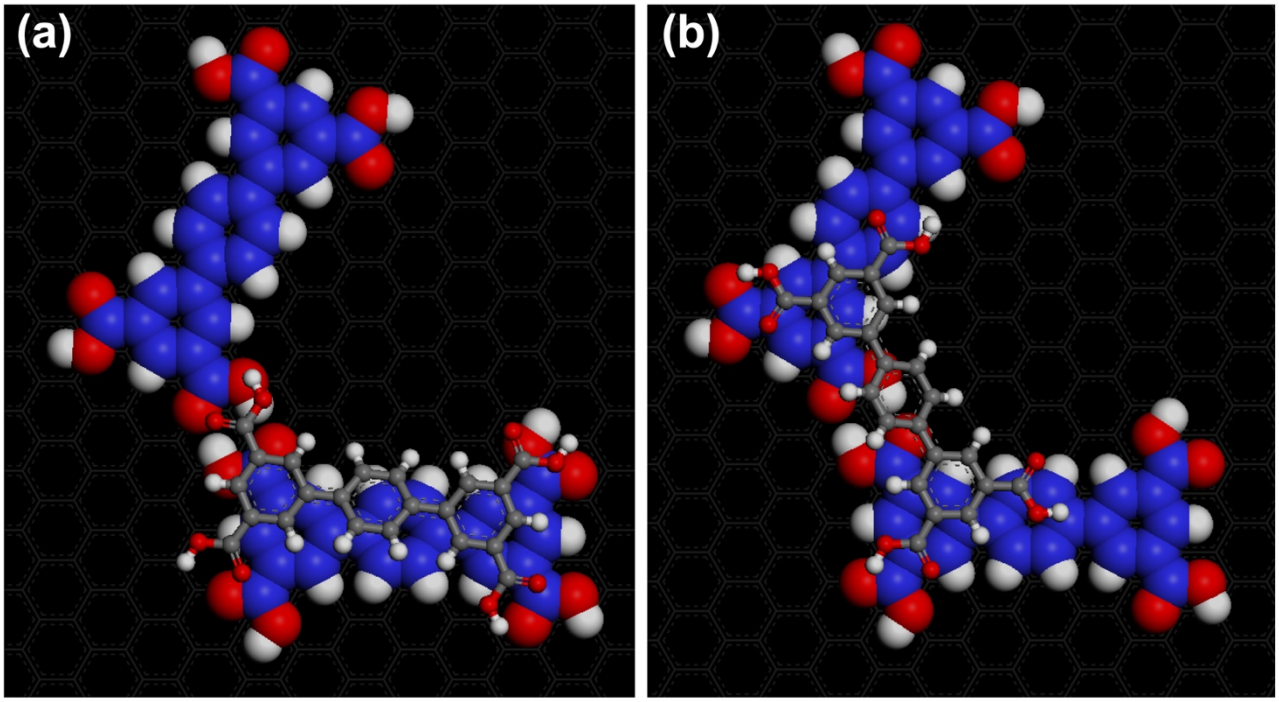

Fig. S14. Adsorption of a **TPTC** molecule (in a balls-and-sticks representation) either on the terphenyl backbone (a) or the H-bonded carboxyl moieties (b) of an arrow head dimer (blue molecules) in the bottom layer. The graphite substrate appears in the background.

The energetic analysis shows that the two adsorption geometries differs in stability by less than 1 kcal/mol, (35.1 kcal mol^{-1} for the geometry in Figure S13a and 34.2 kcal mol^{-1} for the one shown in figure S13b).

As shown in Figure 1C of the manuscript, the length of a **TPTC** molecule is very similar to the distance between the phenyl rings carrying the H-bonded carboxyl groups in the molecules forming an arrow head or parallel dimer, which allows for good molecular registry in both the adsorption geometries discussed here.

The very small difference in the stability suggests that **TPTC** molecules in the top layer do not have strong preferential orientation when adsorbing atop the random tiling network of the **TPTC** monolayer,

which is thus not expected to be able to template and guide the growth of the top layer. Without the templating effect of the bottom layer, we expect the formation of the top layer to be governed by entropy and the resulting bilayer is the stack of two different **TPTC** random tiling networks. Thus, statistically, finding a perfect terphenyl backbone superposition would be a rare event compared to all the other possible adsorption geometries, where the adsorbed molecule sits on the H-bonded carboxyl moieties of the interacting **TPTC** in the bottom layer.

To test that hypothesis, we 'copy-pasted' a typical **TPTC** trimer from the monolayer and adsorbed it in a number of different ways on top of that layer (Figure S15).

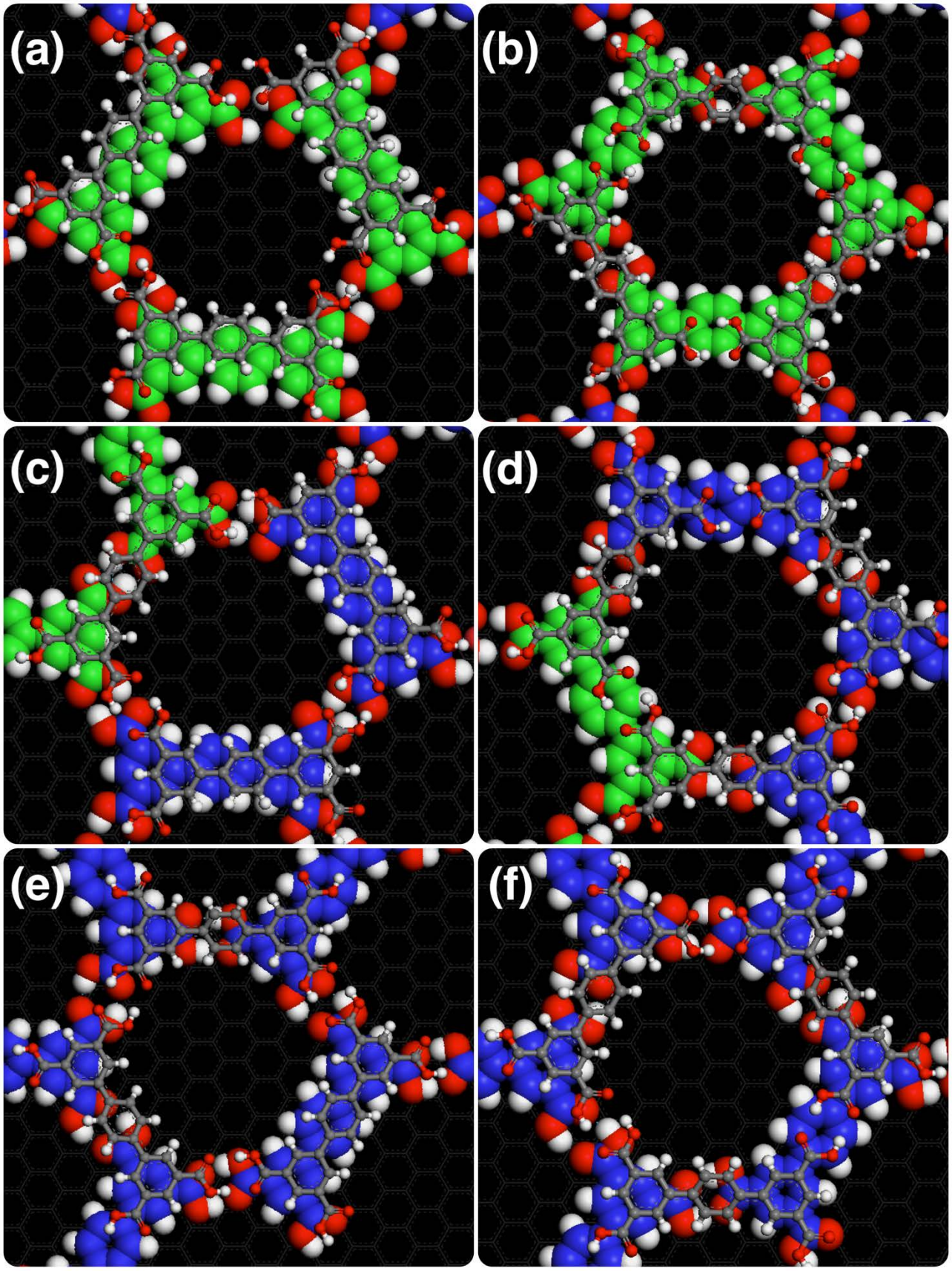

Figure S15. Models used to investigate different adsorption configurations of a **TPTC** trimer over the bottom layer. The molecules shown with "VdW" representations are in the bottom layer, while those with a "ball and stick" representation form the trimer in the top layer. The green molecules are those used to build the **TPTC** trimer for the top layer. The graphite substrate appears in the background.

For the system in Figure S15a, we placed the **TPTC** trimer over a trimer with the same structure, with a perfect superposition of the **TPTC** terphenyl backbones. In Figure S15b, the trimer is rotated 60° over the monolayer, so that now all the **TPTC** molecules in the trimer sit over the H-bonded carboxyl moieties below. For the other systems, the trimer is placed over assemblies in the monolayer composed by 4 (Figure S15c-d) and 5 (Figure S15e-f) interacting molecules, with different orientations. For each system, the adsorption energy has been calculated as the energy difference between the total potential energy of the bilayer and the sum of the potential energies for the non-interacting monolayer (adsorbed on graphite) and the **TPTC** trimer. The results are shown in Table S16.

Table S1. Adsorption energies calculated for the different systems shown in Figure S15.

System	Adsorption Energy (kcal mol^{-1})
S15a	-93.2
S15b	-92.4
S15c	-92.4
S15d	-93.9
S15e	-91.6
S15f	-91.7

As shown in Table S1, the **TPTC** trimer in the top layer interacts favorably with the bottom layer and its adsorption energy, averaged for all the different adsorption sites and orientations, $\langle E_{ads} \rangle$, is $\langle E_{ads} \rangle$ = 92.6 ± 0.9 kcal mol^{-1}.

Since the adsorption energies for **TPTC** trimer for all adsorption sites and orientations are within 0.9 kcal mol^{-1}, which is close to the thermal energy at room temperature K_bT = 0.6 kcal mol^{-1}, the calculations indicate that the bottom layer does not template the formation of the top layer. In turn, this implies that the bilayer can be seen as a stack of two different **TPTC** random tiling networks. Perfect registry between the molecules in the two layers is therefore rather unlikely, which is consistent with the experimental observation that only a minority of the molecules in the top layer have their terphenyl backbone aligned and superposed to that of a **TPTC** molecule in the bottom layer.

Reference:

1. M. O. Blunt, J. C. Russell, M. d. C. Gimenez-Lopez, N. Taleb, X. Lin, M. Schröder, N. R. Champness and P. H. Beton, *Nat. Chem.*, 2011, **3**, 74-78.
2. A. J. J. Lennox and G. C. Lloyd-Jones, *Chem. Soc. Rev.*, 2014, **43**, 412-443.
3. E. M. Campi, W. R. Jackson, S. M. Marcuccio and C. G. M. Naeslund, *Journal of the Chemical Society, Chemical Communications*, 1994, DOI: 10.1039/C39940002395, 2395-2395.